Toward a Practical Demonstration of Physics-Based Beam Calibration Models – CBFPs and the LOFAR-LBA Antenna Array Radio Telescope

A. Young* T. Carozzi† R. Maaskant‡ M. V. Ivashina‡ D. B. Davidson*

***Abstract* — We consider the application of the Characteristic Basis Function Pattern (CBFP) method to calibrate for direction-dependent gain effects of the LOFAR Low Band Antenna (LBA) array. The use of array-based calibration models, as opposed to element-based calibration models, is proposed in order to reduce the number of solvable beam model parameters.**

1 INTRODUCTION

Aperture array radio telescopes, such as LOFAR [1, 2] and the SKA-low [3], face unique calibration challenges due to the wide Field-of-View (FoV) of the elements used in these arrays as well as the long baselines between the different stations comprising the entire instrument. Producing high quality images of the radio sky with instruments such as these will require the application of direction-dependent calibration techniques that are capable of compensating variations in propagation conditions and undesired instrumental gain effects over the FoV [4].

Recently, a number of methods aimed at solving for the direction-dependent gain effects of antennas have been proposed [5, 6]. The common denominator in these methods is the reliance on *a priori* knowledge of the antenna obtained through detailed numerical simulations which, due to advances in computer technology and computational algorithms, are able to analyze large and complex electromagnetic structures. One pattern modeling method in particular, the Characteristic Basis Function Pattern (CBFP) method [6], employs radiation pattern basis functions that are optimally formed to compensate for specific anticipated variations caused by instrumental imperfections.

Herein, the initial application results of the CBFP method are examined to calibrate for direction-dependent gain effects of the LOFAR LBA station at the Onsala Radio Observatory in Sweden.

*Department of Electrical and Electronic Engineering, Stellenbosch University, Stellenbosch, South Africa; e-mail: ayoung@sun.ac.za and davidson@sun.ac.za

†Department of Earth and Space Sciences, Chalmers University of Technology, Gothenburg, Sweden; email: tobia@chalmers.se

‡Department of Signals and Systems, Chalmers University of Technology, Gothenburg, Sweden; email: rob.maaskant@chalmers.se and marianna.ivashina@chalmers.se

2 ARRAY OVERVIEW

Figure 1: The LBA LOFAR station at Onsala with a close-up of one of the inverted-V crossed dipole antennas.

The LOFAR station at Onsala consists of two spatially separated antenna arrays: the Low Band Antenna (LBA) array operating over the 10–90 MHz frequency band and the High Band Antenna (HBA) array operating over 110–240 MHz [2]. The present work is concerned with the LBA array, which consists of 96 crossed dipole antennas arranged in an irregular array. The separation distance between individual antennas in the array ranges from around 3.2 up to about 63.27 m, which is equivalent to about 0.108λ to 16.87λ over

978-1-4673-5710-4/13/$31.00 ©2013 IEEE

the operating frequency band.

Fig. 1 shows a photo of a part of the LBA array, with one of the inverted-V crossed dipole antennas in the foreground. The ends of the dipole arms, each of which has a length of 1.38 m and is oriented at 45° relative to ground, are attached to rubber springs and polyester ropes to form guy wires that keep the antenna upright [7]. Each antenna is positioned above a metal ground plane mesh. High input impedance LNAs for the two dipoles (two polarizations) of each antenna are housed inside the sealed casing at the top of the antenna structure. The output signals of the LNAs are transported via a coaxial cable down below the ground through a polyvinyl chloride (PVC) support structure entering the array processing room.

3 BEAM CALIBRATION MODEL

The open-circuit voltage $v_{\mathrm{oc},i}$ across the terminals of the ith element due to a plane-wave with electric field $\mathbf{e}_j$ that is incident from direction Ω_j can be related to the normalized antenna far-field function $\mathbf{f}_i(\Omega)$ through

$$\begin{aligned} v_{\mathrm{oc},i} &= \mathbf{e}_j \cdot \mathbf{f}_i(\Omega_j) \\ &= e_{\mathrm{cp},j} f_{\mathrm{cp},i}(\Omega_j) + e_{\mathrm{xp},j} f_{\mathrm{xp},i}(\Omega_j) \end{aligned} \tag{1}$$

where the subscripts cp and xp are used to indicated co-polarized and cross-polarized components, respectively. If the voltages of all elements in the array are stacked in a column vector, then the result for N_j different source directions can be written as

$$\begin{aligned} \mathbf{v}_{\mathrm{oc}} &= \sum_{j=1}^{N_j} e_{\mathrm{cp},j} \mathbf{f}_{\mathrm{cp}}(\Omega_j) + e_{\mathrm{xp},j} \mathbf{f}_{\mathrm{xp}}(\Omega_j) \\ &= \mathbf{F}_{\mathrm{cp}} \mathbf{e}_{\mathrm{cp}} + \mathbf{F}_{\mathrm{xp}} \mathbf{e}_{\mathrm{xp}} \end{aligned} \tag{2}$$

where the ijth entry in $\mathbf{F}_{\mathrm{cp}}$ ($\mathbf{F}_{\mathrm{xp}}$) is the co-polarized (cross-polarized) component of the far-field pattern of element i towards the direction of source j, and the jth element in $\mathbf{e}_{\mathrm{cp}}$ ($\mathbf{e}_{\mathrm{xp}}$) is the co-polarized (cross-polarized) component of the incident field due to the source j. Given the antenna impedance matrix $\mathbf{Z}_A$, as well as the LNA impedance matrix $\mathbf{Z}_L$ and voltage gain (typically diagonal) matrix[1] $\mathbf{G}$, the signal presented to the input of the correlator is

$$\mathbf{s} = \mathbf{v} + \mathbf{n}, \tag{3}$$

where $\mathbf{n}$ is additive noise, which is assumed to be statistically independent from $\mathbf{v}$, and

$$\mathbf{v} = \mathbf{G}\mathbf{Z}_L \left(\mathbf{Z}_L + \mathbf{Z}_A\right)^{-1} \mathbf{v}_{\mathrm{oc}} = \mathbf{Q}\mathbf{v}_{\mathrm{oc}}. \tag{4}$$

[1]The amplitude and phase effects of the cable connecting the LNA output to the receiver unit input may be subsumed into this term.

Finally, one of the LOFAR operational modes allows the measurement of the correlation matrix $\mathbf{R}_{\mathrm{s}} = \mathrm{E}\left\{\mathbf{s}\mathbf{s}^H\right\}$, where $\mathrm{E}\{\cdot\}$ denotes expectation. Hence, in terms of the above model, $\mathbf{R}_{\mathrm{s}}$ is computed through (2) and (4) as

$$\begin{aligned} \mathbf{R}_{\mathrm{s}} &= \mathbf{Q} \begin{bmatrix} \mathbf{F}_{\mathrm{cp}} & \mathbf{F}_{\mathrm{xp}} \end{bmatrix} \mathbf{B} \begin{bmatrix} \mathbf{F}_{\mathrm{cp}} & \mathbf{F}_{\mathrm{xp}} \end{bmatrix}^H \mathbf{Q}^H + \mathbf{R}_{\mathrm{n}} \\ &= \mathbf{P}\mathbf{B}\mathbf{P}^H + \mathbf{R}_{\mathrm{n}} = \mathbf{R}_{\mathrm{v}} + \mathbf{R}_{\mathrm{n}} \end{aligned} \tag{5}$$

where the source brightness distribution over the sky is contained in

$$\mathbf{B} = \mathrm{E}\left\{ \begin{bmatrix} \mathbf{e}_{\mathrm{co}}\mathbf{e}_{\mathrm{co}}^H & \mathbf{e}_{\mathrm{co}}\mathbf{e}_{\mathrm{xp}}^H \\ \mathbf{e}_{\mathrm{xp}}\mathbf{e}_{\mathrm{co}}^H & \mathbf{e}_{\mathrm{xp}}\mathbf{e}_{\mathrm{xp}}^H \end{bmatrix} \right\}. \tag{6}$$

All instrumental (and atmospheric) effects distorting the signals of interest are encapsulated in the matrix $\mathbf{P}$. The objective is to find a suitable parametrization for $\mathbf{P}$ which is sufficiently flexible and, at the same time, requires a minimum number of degrees-of-freedom to ease the solving for the free model parameters during a calibration procedure. Following the CBFP approach, solutions for $\mathbf{P}$ are generated, i.e., $\mathbf{P}_1, \mathbf{P}_2, \ldots$, through numerical simulations and/or measurements of the antenna system under various anticipated operating conditions, e.g. by varying amplifier gains or impedances, electrical properties of dry/wet ground, and so forth. Accordingly, let the resulting model $\tilde{\mathbf{P}}$ take the form

$$\tilde{\mathbf{P}} = \sum_{k=1}^{K} \alpha_k \mathbf{P}_k \tag{7}$$

in which the set of weighting coefficients $\{\alpha_k\}_{k=1}^K$ are the solvable parameters. A solution to (7) may be obtained by solving the non-linear minimization problem

$$\boldsymbol{\alpha}_{\mathrm{sol}} = \underset{\boldsymbol{\alpha}}{\mathrm{argmin}} \left\| \tilde{\mathbf{P}}\hat{\mathbf{B}}\tilde{\mathbf{P}}^H - \mathbf{R}_{\mathbf{v}} \right\|_F \tag{8}$$

in which $\hat{\mathbf{B}}$ is based on knowledge of the brightness distribution on the sky, which is updated iteratively as part of the calibration/imaging process [8]. Note that the solution to (8) requires also an accurate estimate of the noise correlation matrix[2] $\mathbf{R}_{\mathrm{n}}$, which may be subtracted from the measured correlation matrix in (5) to yield $\mathbf{R}_{\mathrm{v}}$.

4 NUMERICAL RESULTS

The entire LOFAR LBA array was analyzed in FEKO [9] to compute the open-circuit Embedded Element Patterns (EEPs), which are shown in

[2]The characterization of noise present in the system, specifically that produced by the LNAs, is the focus of ongoing work.

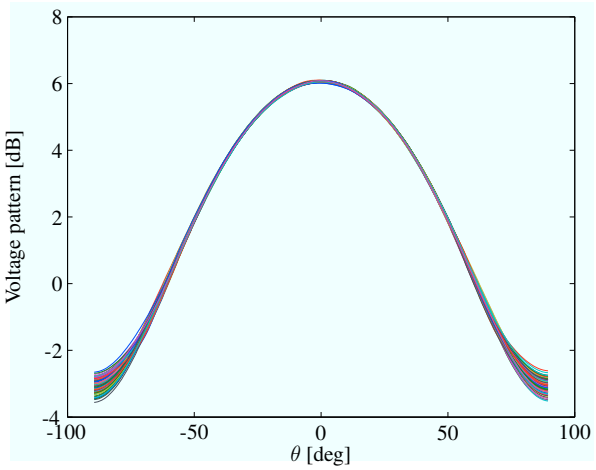

(a) 40 MHz

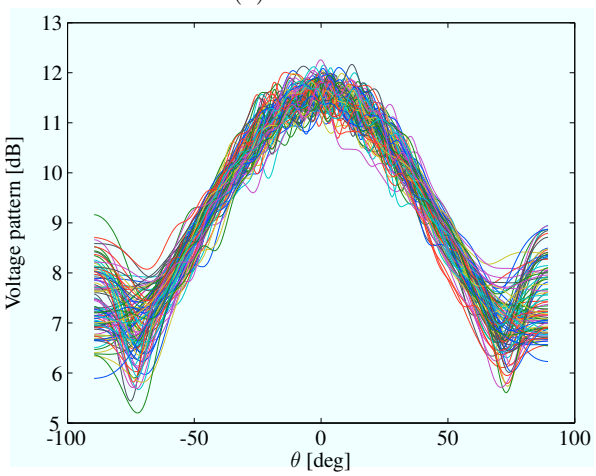

(b) 70 MHz

Figure 2: Co-polarized embedded element patterns of all 96 x-oriented dipoles in $\phi = 0°$ plane.

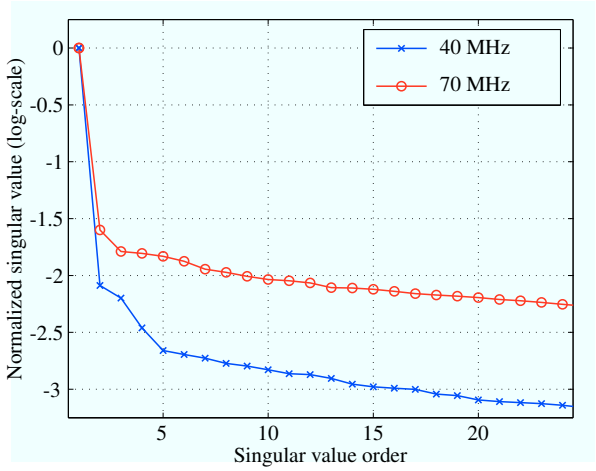

Figure 3: Singular value spectra for the set of embedded element patterns at two frequencies. Each spectrum is normalized to the maximum singular value.

Fig. 2. Note that the element patterns are very similar at lower frequencies, whereas the pattern variability among the elements increases at large frequencies.

In order to emphasize the impact of the pattern variability exhibited in Fig. 2 on the DOFs for beam modeling, consider constructing a small set of basis functions for modeling each of the patterns shown. One approach is to stack each of the angular discretized patterns as columns in a matrix which is then subject to the Singular Value Decomposition (SVD), after which the left singular vectors corresponding to Singular Values (SVs) above a certain threshold are used as basis functions [10]. The SV spectra corresponding to the patterns in Fig. 2 were computed and are shown in Fig. 3. In this case only the co-polarized patterns of the x-oriented elements were used. The patterns were sampled over a regular grid in (θ, ϕ)-space, resulting in a denser spatial sampling around zenith than lower on the horizon, and a weighting scheme was applied to compensate for this. By retaining only basis functions corresponding to (normalized) SVs above 10^{-3} yields a 16-parameter model for each of the patterns at 40 MHz and a 96-parameter model at 70 MHz. Even when the threshold increased to a value of 10^{-2} — and thus allowing a loss in accuracy — an 8-parameter model is still required for each of the patterns at 70 MHz. In either case, multiplying the number of parameters per pattern with the number of elements in the array results in a large number of parameters to solve.

As opposed to modeling each element pattern individually, the method outlined in Sec. 3 produces a model for all the element patterns in the entire array simultaneously. This implies that DOFs are not wasted for modeling the effects of mutual coupling (i.e. the variability among patterns of different elements in the array), which are deterministic and could be taken into account using simulated and/or measured results. Furthermore, the gain and impedance loading effects of the LNAs are also incorporated in that approach, so that these effects may not increase the calibration complexity significantly either. A study to determine the efficiency of the proposed modeling technique is underway.

5 CONCLUSION

A procedure to apply the CBFP method to the direction-dependent gain calibration effects of large aperture antenna arrays has been described. With the goal of minimizing the number of free parame-

ters that need to be solved during such calibration procedure, the use of array-based models instead of element-based models was motivated.

Ongoing work is focused on the detailed characterization of the LOFAR LBA station at Onsala through the direct measurement of the system, the implementation of the above-described calibration technique, and the subsequent application of the method to the measured data in order to obtain an enhanced image of the actual source distribution on the sky.

Acknowledgments

The authors acknowledge the support of SKA South Africa, the South African Research Chairs Initiative of the Department of Science and Technology (DST), the National Research Foundation (NRF), and the Swedish Vinnova and VR grants.

References

[1] M. De Vos, A. Gunst, and R. Nijboer, "The LOFAR Telescope: System Architecture and Signal Processing," *Proc. IEEE*, vol. 97, no. 8, pp. 1431–1437, Aug. 2009.

[2] S. Wijnholds, W. van Cappellen, J. bij de Vaate, and A. van Ardenne, "Antenna applications corner: Phased-array antenna system development for radio-astronomy applications," *IEEE Antennas Propag. Mag.*, vol. 55, no. 6, pp. 293–308, Dec. 2013.

[3] P. E. Dewdney, P. J. Hall, R. T. Schilizzi, and T. J. L. W. Lazio, "The Square Kilometre Array," *Proc. IEEE*, vol. 97, no. 8, pp. 1482–1496, Aug. 2009.

[4] S. J. Wijnholds, S. van der Tol, R. Nijboer, and A. van der Veen, "Calibration challenges for future radio telescopes," *Signal Processing Magazine, IEEE*, vol. 27, no. 1, pp. 30–42, 2010.

[5] C. Craeye, D. Gonzalez-Ovejero, N. R. Ghods, and E. de Lera Acedo, "A Projection Approach to Model the Main Beam of Non-Regular Arrays in Presence of Mutual Coupling," in *Proc. EuCAP*, Mar. 2012, pp. 2609–2612.

[6] R. Maaskant, M. V. Ivashina, S. J. Wijnholds, and K. F. Warnick, "Efficient Prediction of Array Element Patterns Using Physics-Based Expansions and a Single Far-Field Measurement," *IEEE Trans. Antennas Propag.*, vol. 60, no. 8, pp. 3614–3621, Aug. 2012.

[7] W. A. van Cappellen, M. Ruiter, and G. W. Kant, "Low Band Antenna Architectural Design Document," ASTRON, Tech. Rep., Mar. 2007.

[8] O. M. Smirnov, "Revisiting the radio interferometer measurement equation. II. Calibration and direction-dependent effects," *Astronomy & Astrophysics*, vol. 527, p. A107, 2011.

[9] EM Software & Systems S.A. (Pty) Ltd, FEKO, Suite 6.3. [Online]. Available: http://www.feko.info

[10] A. Young, R. Maaskant, M. V. Ivashina, D. I. L. de Villiers, and D. B. Davidson, "Accurate Beam Prediction Through Characteristic Basis Function Patterns for the MeerKAT/SKA Radio Telescope Antenna," *IEEE Trans. Antennas Propag.*, vol. 61, no. 5, pp. 2466–2473, May 2013.